Quantum criticality preempted by nematicity

Shi-Xin Zhang,[1] Shao-Kai Jian,[1,2] and Hong Yao[1,3,*]
[1]*Institute for Advanced Study, Tsinghua University, Beijing 100084, China*
[2]*Department of Physics, Harvard University, Cambridge, Massachusetts 02138, USA*
[3]*State Key Laboratory of Low Dimensional Quantum Physics, Tsinghua University, Beijing 100084, China*

(Received 11 October 2018; accepted 13 April 2021; published 22 April 2021)

Exotic physics often emerges around quantum criticality in metallic systems. Here we explore the nature of topological phase transitions between 3D double-Weyl semimetals and insulators (through annihilating double-Weyl nodes with opposite chiralities) in the presence of Coulomb interactions. From renormalization-group (RG) analysis, we find a non-Fermi-liquid quantum critical point (QCP) between the double-Weyl semimetals and insulators when artificially neglecting short-range interactions. However, it is shown that this non-Fermi-liquid QCP is actually *unstable* against nematic ordering when short-range interactions are correctly included in the RG analysis. In other words, the putative QCP between the semimetals and insulators is preempted by the emergence of nematic phases when Coulomb interactions are present and thus double-Weyl fermions cannot directly annihilate with each other. We further discuss the possible experimental relevance of the nematicity-preempted QCP to double-Weyl candidate materials $HgCr_2Se_4$ and $SrSi_2$.

DOI: 10.1103/PhysRevB.103.165129

I. INTRODUCTION

Quantum critical phenomena are long-standing topics in condensed-matter physics as universal properties and exotic physics often emerge near quantum critical points (QCPs) [1–6]. Nonetheless, under certain circumstances, a QCP could be preempted by another symmetry-breaking phase, e.g., superconductivity as shown in Fig. 1(a), such that the universal non-Fermi-liquid (NFL) properties controlled by the putative QCP can only been measured in the critical regime *outside* the preempting phase. Experimental evidence of such QCPs preempted by superconductivity has been reported in various systems including high-temperature superconductors (for a review, see, e.g., Refs. [7,8]). Interesting aspects of the interplay between strong fluctuations of QCPs and emergent preempting phases in metallic systems with large Fermi surfaces have been extensively studied theoretically (see, e.g., Refs. [9–22]). However, novel features of preempted QCPs in topological semimetals remain largely unexplored.

Topological semimetals feature band-crossing points in momentum space, which are protected by their topological characters and/or crystalline symmetries [23–37]. It has been known that correlation effects in ideal topological semimetals with only discrete points at the Fermi level should be qualitatively different from the usual systems with large Fermi surfaces [38] because of the vanishing density of states in ideal topological semimetals. Systems hosting discrete Fermi points with either short-range interactions [39–47] or long-range Coulomb interactions [48–50] have been extensively studied in the past decade, showing various behaviors such as NFL states [51–54], topological Mott insulators [55–58], anisotropic screening of Coulomb interactions [59–65], fermion-induced QCPs [66–71], and even emergent space-time supersymmetry [72–78].

The family of topological semimetals includes multi-Weyl semimetals hosting double-Weyl (triple-Weyl) fermions with ± 2 (± 3) monopole charge of Berry curvature in momentum space, which are generalizations of Weyl fermions with monopole charge ± 1 [79–84]. Topological phase transitions between the topological semimetals and insulators are generally believed to be a result of the annihilation of Weyl or multi-Weyl nodes. In this paper, we show how the simple picture of annihilation between Weyl fermions in condensed matter systems is qualitatively modified by the correlation behaviors around such topological QCPs.

Here we investigate the nature of putative topological phase transitions between double-Weyl semimetals (DWSs) and (trivial or Chern) insulators in the presence of Coulomb interactions. We focus on intriguing aspects such as possible mechanism to preempt such putative QCPs and the consequence of avoided annihilation between double-Weyl fermions. In the presence of long-range Coulomb interactions, our renormalization-group (RG) analysis shows that the QCP is stable, exhibiting NFL behaviors when short-range interactions that allowed by symmetry are *artificially* neglected. However, we find that this putative NFL QCP is unstable when short-range interactions are *correctly* included in the RG analysis. Specifically, the putative QCP is preempted by emergent nematic phases [85] that are induced collaboratively by long-range and short-range interactions. Around the putative QCP, the long-range part of the Coulomb interaction induces strong nematic susceptibility and nematicity emerges when short-range interactions are correctly taken into account, preempting the putative QCP as shown in Fig. 1(b).

*yaohong@tsinghua.edu.cn

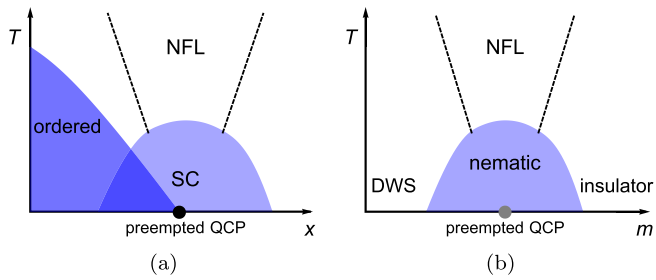

FIG. 1. Schematic phase diagrams of QCPs preempted by superconductivity (a) and by nematicity (b). In (b), the QCP is preempted by nematicity in the presence of Coulomb interactions. x and m represent tuning parameters such as doping level and magnetic field, and T refers to temperature. NFL denotes non-Fermi liquid, SC superconductivity, and DWS double-Weyl semimetals.

II. THE MODEL

We consider a two-band model of noninteracting fermions on a cubic lattice exhibiting topological phase transitions between double-Weyl semimetals and insulators:

$$H_0 = \sum_{\mathbf{k}} c^\dagger_{\mathbf{k}}[2t_1(\cos k_y - \cos k_x)\sigma_x + 2t_2 \sin k_x \sin k_y \sigma_y + t_3(6 - 2\cos k_x - 2\cos k_y - 2\cos k_z + m)\sigma_z]c_{\mathbf{k}}, \quad (1)$$

where σ_i are Pauli matrices representing orbital degrees of freedom, $c^\dagger_{\mathbf{k}\alpha}$ create spin-polarized electrons in $\alpha = 1, 2$ orbitals, and t_j with $j = 1, 2, 3$ denote various hopping amplitudes. We have set the lattice constant to one for simplicity and we assume $t_1 = t_2$ hereafter as their difference is not essential to our discussions below. The parameter m can be tuned by experimental knobs such as pressure or magnetic field to access different phases, including DWSs, three-dimensional (3D) Chern insulators (CIs), and trivial band insulators (BIs). The quantum phase diagram of this noninteracting Hamiltonian as a function of m is shown as Fig. 2. The Hamiltonian in Eq. (1) respects C_{4h} symmetries apart from translational symmetries. In the DWS phase, it is the C_4 rotational symmetry around the z axis that protects the double-Weyl fermions; the mirror symmetry ($z \to -z$) requires the two double-Weyl nodes to have the same energy.

As shown in Fig. 2, $m = 0, -4$ represent the noninteracting QCPs between DWSs and insulators (BI or CI). The QCPs realize quadratic band touching (QBT). Note that the QBT at the QCP is still anisotropic between k_x/k_y and k_z directions due to the lack of cubic symmetry. We call QBT fermions at such QCPs as critical quadratic fermions (CQFs). They are critical states achieved by fine-tuning some parameter, say m in the present case. Therefore, CQF is qualitatively different from stable 3D QBT systems, such as pyrochlore iridates and α-Tin, which are protected by O_h point-group symmetry

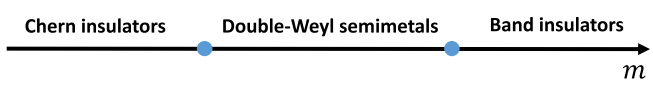

FIG. 2. The quantum phase diagram with varying m for the model in Eq. (1).

and described by the Luttinger Hamiltonian with isotropic dispersions [86]. We shall focus on the QCP at $m = 0$ below, and the same physics applies to the critical point between the DWS and CI.

The QCP of noninteracting fermions in Eq. (1) is stable against weak short-range interactions because of the vanishing density of states at Fermi level (see Appendix for details). However, since the density of states at the Fermi level vanishes, the Thomas-Fermi mechanism may fail to sufficiently screen Coulomb interactions. We need to carefully investigate whether Coulomb interactions are effectively screened or not in such systems, especially at the putative QCP between the DWS and the insulator. As pointed out in previous works [62,63], deep in the DWS phase, the strength of the long-range tail of Coulomb interactions is marginally irrelevant, rendering the DWS a marginal Fermi liquid. However, CQFs have larger densities of states in low energy, which is expected to be more susceptible to interactions than double-Weyl fermions. Therefore, it is desired to study the fate of a CQF in the presence of Coulomb interactions by performing RG analysis.

III. RG ANALYSIS OF PREEMPTED QCP

It is worth noting that as long as there is finite long-range Coulomb interaction, short-range interactions can be generated at low energy even when their bare values are zero. This is because the short-range four-fermion interaction can be generated at the one-loop level from long-range Coulomb interaction (see Appendix for details). Therefore, one needs to consider both long-range interactions as well as short-range interactions simultaneously at the beginning, and see how the interplay between long-range and short-range interactions affects the QCP in question.

We are ready to write down the effective field theory in the continuum including both long-range and short-range parts of the Coulomb interaction. The long-range part of the Coulomb interaction can be represented by introducing a boson field ϕ. The (Euclidean) action at the putative QCP is then given by

$$S = \int \frac{d^3k d\omega}{(2\pi)^4}\left[\psi^\dagger_{\mathbf{k}}(i\omega + \mathcal{H}_{0\mathbf{k}})\psi_{\mathbf{k}} + \frac{1}{2}\phi_{\mathbf{k}}\left(k_x^2 + k_y^2 + \eta k_z^2\right)\phi_{-\mathbf{k}}\right] + \int d^4x[ie\phi\psi^\dagger\psi + g(\psi^\dagger\psi)^2], \quad (2)$$

where $\mathcal{H}_{0\mathbf{k}} = t_1(k_x^2 - k_y^2)\sigma_x + 2t_2 k_x k_y \sigma_y + t_3 k_z^2 \sigma_z$ represents the low-energy effective Hamiltonian of the noninteracting lattice model at the QCP ($m = 0$ or 4), and e and g stand for the strength of long-range Coulomb interaction and short-range interactions (there is only one independent on-site four-fermion interaction term), respectively. Note that the parameter $\eta > 0$ is introduced in the kinetic term of boson fields to reflect the generic anisotropy of Coulomb potentials between the x/y and z directions. The hopping parameters t_1 and t_2 are, in general, different as the lattice system respects only the discrete C_4 rotational symmetry. When $t_1 = t_2$, a U(1) rotational symmetry in the xy plane emerges in the low-energy effective action in Eq. (2).

We then perform RG analysis of the effective theory in Eq. (2) to derive critical behaviors of the putative QCP in the presence of Coulomb interaction. We set the scaling

dimensions $[\omega] = 1$, $[k_{x,y}] = z_1$ and $[k_z] = z_3$ to keep the noninteracting part invariant under RG. The tree-level values are $z_1 = z_3 = 1/2$ due to the quadratic dispersion. In general, z_1 and z_3 are different due to the anisotropy between x/y and z directions. We obtain z_1, z_3 by requiring t_1 and t_3 fixed (namely, the flow equations for t_i equal zero) in RG. In addition, we carry out the RG analysis in different dimensions to control the approximation—namely, we implement the calculation in spatial dimension $d = 4 - \epsilon$, where $d = 4$ is the upper critical dimension and $\epsilon = 1$ corresponds to the realistic systems. The remaining RG equations for various parameters in the action are given by

$$\frac{de}{dl} = \left(-\frac{z_3}{2} + \frac{1}{2} - \frac{\eta_\phi}{2} - \frac{1-\epsilon}{2} z_1 \right) e, \tag{3}$$

$$\frac{d\eta}{dl} = (2z_1 - 2z_3 - \eta_\phi)\eta + F_\eta, \tag{4}$$

$$\frac{dg}{dl} = (1 - (3-\epsilon)z_1 - z_3)g + F_1 g^2 + F_2 g e^2 + F_3 e^4, \tag{5}$$

where $\eta_\phi/2$ is the anomalous dimension of the boson field ϕ and F_i are some numerical functions derived from Feynman diagram amplitude (see the details in Appendix).

When the long-range part of Coulomb interaction is not present ($e = 0$), it is clear that the short-range interaction g is irrelevant at the Gaussian QCP between the semimetals and insulators (the tree-level scaling for g is $[g] = -1/2$). When $e > 0$, the system may fail to screen the long-range Coulomb interaction effectively due to the vanishing density of the states at the putative QCP. As a consequence, the long-range Coulomb interaction can render nontrivial correlation effects at the putative Gaussian QCP as we analyze below.

When $e > 0$, it turns out that short-range interaction g cannot be neglected in the RG analysis even when its bare value is zero ($g_0 = 0$). This is because the long-range part of the interaction can generate short-range interaction g under RG flow, as clearly shown in Eq. (5). However, if one *artificially* restricts RG flows within the parameter space of $g = 0$, one obtains an exotic QCP which corresponds to a NFL fixed point characterized by anisotropic Coulomb interaction given by $e \neq 0$ and $\eta \approx 2/3$ (see Appendix for details). This NFL QCP, obtained by requiring $g_0 = 0$ and artificially neglecting the flow of g, is marked as the red point in the $g = 0$ plane, as shown in Fig. 3. Note that e is relevant in this case, and we need to investigate the system carefully by lowering the dimension from the marginal dimension $d = 4$ for Coulomb interactions, the detailed justifications based on dimension can be found in the Appendix.

However, the putative NFL fixed point in the $g = 0$ plane is actually unstable once the short-range interaction g is correctly allowed to flow under RG, as shown by the runaway trajectory in Fig. 3. Since the short-range interaction is allowed by symmetry, its bare value g_0 is in general nonzero. Even when its bare value is fine tuned to zero, it is inevitably generated by the long-range part e of the Coulomb interaction and even infinitesimal long-range Coulomb interactions are able to drive the flow of the short-range interaction to strong-coupling limit. Such a runaway flow of g can also be further convinced by a fixed point collision picture (see details in the Appendix). The runaway RG flow of short-range interactions implies that a certain type of symmetry breaking should occur around the putative QCP although the RG flow itself cannot tell which type of ordering actually is induced. After knowing the relevant interactions under the RG flow, one can employ the self-consistent mean-field calculations to obtain the pattern of symmetry breaking. We find that the putative Gaussian QCP between the semimetals and insulators is destroyed and intermediate nematic phases emerge between the semimetals and insulators. In other words, the presumed QCP is preempted by nematicity and the direct annihilation between double-Weyl fermions is forbidden.

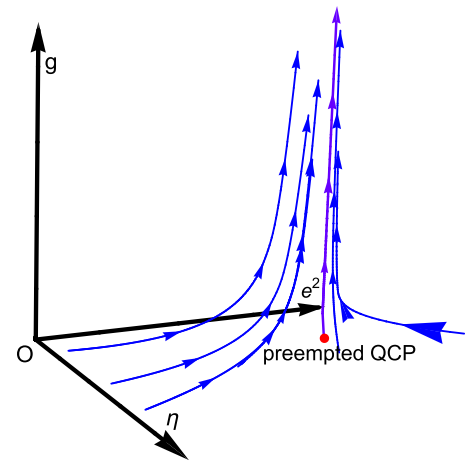

FIG. 3. The RG flow diagram of the critical quadratic fermions with both short-range and long-range interactions. The red point stands for the NFL fixed point when we artificially discard short-range interactions in RG analysis. It is clear all flows lead to strong coupling of short-range interaction g as long as $e > 0$, which preempts the presumed QCP with the NFL fixed point.

IV. THE QUANTUM PHASE DIAGRAM

Since the QCP is shown to be preempted by nematic ordering, a natural question is how low-energy physics near the QCP gets modified. For double-Weyl fermions near the presumed QCP, the separation of two double-Weyl nodes at $\pm\mathbf{k}^* = (0, 0, \pm\sqrt{|m|})$ is small. Before the annihilation of double-Weyl nodes, the low-energy physics of the system is captured by the interplay between long-range Coulomb and short-range interaction of the double-Weyl fermions.

The Hamiltonian of the double-Weyl fermion around $\mathbf{k}^*_\pm$ in continuum can be deduced from Eq. (1). We first consider the double-Weyl fermion around $+\mathbf{k}^*$. For $|\tilde{k}_z| \ll 2\sqrt{|m|}$ with $\tilde{k}_z = k_z - k^*_z$, one can obtain the following low-energy effective Hamiltonian for the double-Weyl fermion around $+\mathbf{k}^*$: $\mathcal{H}_{\mathrm{DWF},\mathbf{k}} = t(k_x^2 - k_y^2)\sigma_x + 2tk_xk_y\sigma_y + 2\sqrt{|m|}\tilde{k}_z\sigma_z$, where higher order terms in $\tilde{k}_z$ are neglected. The cutoff of the continuous Hamiltonian for double-Weyl fermions is $\Lambda \sim \sqrt{|m|}$. The action of the double-Weyl fermions with both long-range and short-range interactions is similar to the one in Eq. (2), except that the Hamiltonian $\mathcal{H}_{0\mathbf{k}}$ of the CQF is replaced by $\mathcal{H}_{\mathrm{DWF}}$, namely, $\mathcal{H}_{0\mathbf{k}} \to \mathcal{H}_{\mathrm{DWF},\mathbf{k}}$ in Eq. (2). In the DWS phase, it is known that long-range Coulomb interactions are marginally irrelevant at the stable

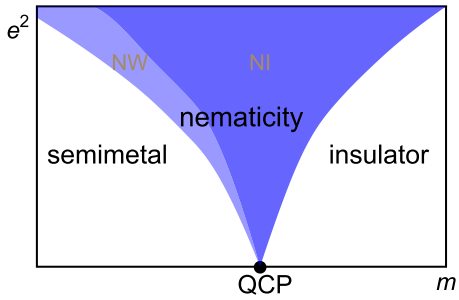

FIG. 4. Quantum phase diagram describing annihilation of double-Weyl fermions in the presence of Coulomb interaction. The putative QCP between (double-Weyl) semimetals and (trivial or Chern) insulators is preempted by nematic phases as long as Coulomb interaction is finite. NI and NW denote nematic insulator and nematic Weyl semimetal, respectively.

fixed point with $e=0, \eta=0$. Consequently, weak Coulomb interaction is unable to drive short-range interactions to strong coupling to destabilize the DWF phase. However, when e exceeds a critical value e^*, it can generate a relevant short-range four-fermion term that drives the system to the strong coupling and then induces a phase transition to the nematic phase. Since the only scale in the system is set by Λ, one expects the critical value for Coulomb interaction to scale as $e^{*2} \sim \Lambda \sim \sqrt{|m|}$ (see Appendix for details). Note that this scaling analysis is consistent with the preempted QCP: $e^* = 0$ for $m = 0$. The obtained schematic quantum phase diagram is shown in Fig. 4.

V. DISCUSSIONS AND CONCLUDING REMARKS

From RG analysis, we obtained a nontrivial picture describing the topological phase transition from 3D DWSs to insulators (including 3D CIs). The conventional picture for this topological phase transition is simple, namely, two double-Weyl nodes with opposite chiralities approach each other and annihilate at a high-symmetry point in the Brillouin zone, rendering a fully gapped insulator after the annihilation. This picture is valid in the absence of long-range Coulomb interaction. However, when the long-range part of Coulomb interaction (even infinitesimal) is taken into account, each double-Weyl node will split into two Weyl points with the same chirality, breaking the lattice C_4 rotational symmetry before annihilation. Then, these split Weyl points with opposite chiralities in the nematic phase can annihilate with one another, resulting in a fully gapped insulator with nematic ordering. Previously, it was widely believed that double-Weyl fermions with opposite chiralities can annihilate directly in solids. This belief is convincingly challenged and negated. The physics of QCPs preempted by nematicity may be understood in the following heuristic way. If two double-Weyl fermions meet, forming CQFs, the density of states at low energy increases, which is in general unfavored when relevant interactions are present and when there are other available phases with a lower density of states. Indeed, by splitting each double-Weyl node into two Weyl nodes, the density of states is lowered such that the splitting is more favored than annihilating directly.

The preempted QCP scenario applies similarly to the presumed topological phase transition between triple-Weyl semimetals with monopole charge ± 3 protected by the C_6 symmetry and insulators. For this case, the long-range Coulomb interaction is relevant and drives the noninteracting critical triple-Weyl fermions to a NFL fixed point, which in return renders short-range interactions relevant. The runaway flow of short-range interactions leads to nematic ordering where each triple-Weyl node is split into three Weyl points breaking the C_6 symmetry down to C_3. Consequently, Weyl fermions with higher monopole charges are forbidden to directly annihilate in realistic systems.

The picture of QCPs preempted by nematicity illustrated above could be closely related to realistic materials hosting ideal multi-Weyl fermions. There are already proposals of candidate materials hosting double-Weyl fermions based on first-principles calculations including $HgCr_2Se_4$ [27] and $SrSi_2$ [32]. We believe that materials realizing ideal double-Weyl or triple-Weyl semimetals is ideal platform to demonstrate the preempted QCP proposed in the present paper. For instance, applying strain, pressure, or magnetic field to such semimetal materials should be able to tune the parameter m and drive them toward insulators. One can measure quantities such as angle-dependent specific heat and angle-dependent resistivity to observe the predicted nematicity before entering symmetry-preserving insulators.

It is worth mentioning some analogies between QCPs preempted by nematicity proposed in the present paper and QCPs preempted by superconductivity observed in superconducting materials. In the latter, when approaching the preempted QCP, the instability toward superconductivity is enhanced by the strong fluctuations around the underlying NFL fixed point, the putative NFL nature of QCP is preempted due to the formation of superconductivity. For the former case studied here, the topological QCP disappears and is replaced by an intermediate nematic phase induced by the enhancement of fluctuations around QCPs. This may shed light to deeper understanding of the interplay between quantum phase transitions and strong correlations in topological states of matter [23,24,87].

ACKNOWLEDGMENTS

We thank S.-E. Han and Eun-Gook Moon for helpful discussions. This work was supported in part by NSFC of China Grant No. 11825404 (S.-X.Z., S.-K.J., and H.Y.), the MOSTC under Grants No. 2016YFA0301001 and No. 2018YFA0305604 (H.Y.), the Strategic Priority Research Program of Chinese Academy of Sciences under Grant No. XDB28000000 (H.Y.), Beijing Municipal Science and Technology Commission under Grant No. Z181100004218001 (H.Y.), and Beijing Natural Science Foundation under Grant No. Z180010 (H.Y.).

APPENDIX

1. The mean-field analysis for short-range interactions

We study the lattice model in the main text with only short-range interactions. In general, on-site short-range interactions in the two-band model can be described as four-fermion interactions with no momentum dependence: $(\psi^\dagger M \psi)(\psi^\dagger N \psi)$

where M, N are two by two Hermitian matrix and $\psi = (c_{1\mathbf{k}}, c_{2\mathbf{k}})$. In our specific systems, by requiring C_4 rotation symmetry protecting double-Weyl nodes and particle-hole symmetry which fix Fermi energy on the Weyl nodes, we are finally left with only four interactions $(\psi\sigma_i\psi)^2$, where σ_i is identity matrix for $i = 0$ and Pauli matrix for $i = 1$ to 3, namely, only those interactions with $M = N$ keep all necessary symmetry in our model. We further utilize the Fierz identity for the two by two matrix as

$$(\psi^\dagger M\psi)(\psi^\dagger N\psi) = -\tfrac{1}{4}(\mathrm{Tr}M\sigma_i N\sigma_j)(\psi^\dagger\sigma_i\psi)(\psi^\dagger\sigma_j\psi). \tag{A1}$$

We can get four equations for interactions where we set $M = N = \sigma_i$ and find the unique solution which satisfies Fierz identity and symmetry requirements. The relation is $(\psi^\dagger\sigma_0\psi)^2 = -(\psi^\dagger\sigma_i\psi)^2$ for $i = 1$ to 3 and we finally reduce ten terms of four-fermion interactions to one independent term. This term is just Hubbard interaction as $2gn_1n_2$, where $n_i = \psi_i^\dagger\psi_i$ is the density for *ith* orbital. We always assume $g > 0$, namely, repulsive Hubbard interaction, and that can be justified by RG analysis, where the only stable runaway flow for a (critical) double-Weyl fermion system is toward $g \to +\infty$.

In the RG sense, the strength of such four-fermion interaction g has scaling dimension -1 in tree level in the double-Weyl fermion case and scaling dimension $-1/2$ in tree level in the critical quadratic Weyl fermion case and hence irrelevant at the Gaussian fixed point representing free (critical) double-Weyl fermions, namely, infinitesimal short-range interactions cannot drive the system to other phases, and only short-range interactions with finite interaction strength exceeding some critical value g_c can induce phase transitions in this system.

Therefore, we apply the mean-field approach to investigate ordered phases induced by short-ranged interactions. In principle, for a two-band model, there are four independent terms for possible orders as $\langle\psi^\dagger\sigma_i\psi\rangle$ in particle-hole channel (particle-particle channel instabilities are not favored since there is always a repulsive interaction). Among them, $\langle\psi^\dagger\sigma_0\psi\rangle$ is just the shift of chemical potential and can be dropped. Similarly, $\langle\psi^\dagger\sigma_3\psi\rangle$ coupled to $\psi^\dagger\sigma_3\psi$ corresponds to the shift of m in the model. However, since we assume m is a controllable external parameter, the renormalization is also omitted. In sum, there are only two remaining order parameters which are responsible for nematic orders breaking C_4 rotation symmetry down to C_2.

We decouple the Hamiltonian with Hubbard interactions as

$$\begin{aligned} H_{\mathbf{mf}} = \sum_{\boldsymbol{k}} & [(\cos k_y - \cos k_x + 2g_1\Delta_1)\sigma_x \\ & + (\sin k_x \sin k_y + 2g_2\Delta_2)\sigma_y \\ & + (6 - 2\cos k_x - 2\cos k_y - 2\cos k_z + m)\sigma_z] \\ & - g_1\Delta_1^2 - g_2\Delta_2^2, \end{aligned} \tag{A2}$$

where $\Delta_i = \langle\psi^\dagger\sigma_i\psi\rangle$ as two order parameters and g_1, g_2 are interaction strengths which obey the constraint $g_1 + g_2 = -g$ from Fierz identity. Our task is to minimize the free energy numerically for each m and g and find corresponding orders $\Delta_{1,2}$. For simplicity, we assume hopping parameters $t_1 = t_2 = t_3 = 1$ in most of the calculations below.

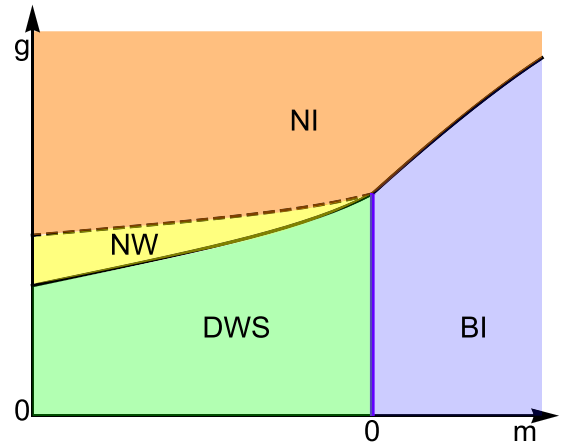

FIG. 5. Mean-field phase diagram with repulsive on-site interactions g: BI: Trivial band insulator or 3D Chern insulator. DWSs: Double-Weyl semimetals hosting two double-Weyl nodes. NW: Nematic Weyl fermion phase. NI: Nematic insulator phase. Black lines represent second-order phase transitions from disorder to nematic order phase. Purple line represents topological phase transition from double-Weyl semimetals to trivial insulators whose low-energy effective theory is critical quadratic fermions (CQFs). Dashed line lies at where nematic Weyl fermions annihilate as AWF.

In our model, when there is nematic order, it always tends to develop a $\Delta_2 \neq 0$ phase while $\Delta_1 = 0$, and this feature is model dependent. It is worth noting that there are different phases corresponding to nematic orders $\Delta_2 \neq 0$. When $0 < g_2\Delta_2 < l_c$, the double-Weyl node split into two Weyl fermions in the xy diagonal directions, forming a nematic Weyl fermion phase; when $g_2\Delta_2 = l_c$, the four Weyl fermions meet with each other on a $k_z = 0$ plane, forming so-called anisotropic Weyl fermions (AWFs); and when $g_2\Delta_2 > l_c$, there is full gap in the system as a nematic insulator.

Similar with CQF, which is formed when two double-Weyl fermions overlap, we have AWFs when $g = g_c'$. An AWF is formed when two single-Weyl fermions overlap and have linear dispersion in two directions and quadratic dispersion in the third momentum direction. An AWF here serves as a critical state separating Weyl semimetal and nematic insulator phases which can also be named as critical Weyl fermions.

The mean-field phase diagram considering short-range interactions is shown in Fig. 5. Apparently, the original scenario for topological phase transitions accomplished by annihilating double-Weyl fermions remains unchanged when short-range interactions are small.

2. RG analysis on CQF with Coulomb interactions

Although short-range interactions are inevitably generated from coarse graining as we show in the next section, we here perform RG considering only Coulomb interactions to see the presumed QCP and related NFL behaviors, which is helpful to understand the physics when short-range interaction are considered: how NFL properties get destroyed and how the QCP is preempted.

Therefore, we carry out RG calculation on CQF systems ($m = 0$) with Coulomb interactions alone; though short-range

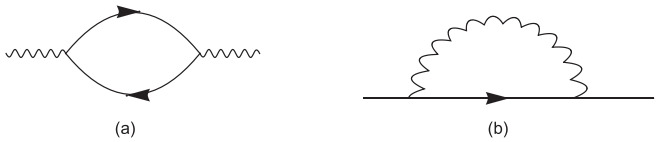

FIG. 6. Feynman diagrams relevant to Coulomb interactions: Solid lines stand for fermions and wavy lines stand for Coulomb potential.

interactions inevitably grow with the energy scale, we omit them in this section. The action is captured by

$$S = S_\psi + S_\phi + S_e, \tag{A3}$$

$$S_\psi = \frac{1}{(2\pi)^4}\int d^3k d\omega\ \psi^\dagger_{\mathbf{k}}(-i\omega + H_l(m=0))\psi_{\mathbf{k}}, \tag{A4}$$

$$S_\phi = \frac{1}{(2\pi)^4}\int d^3k d\omega\ \frac{1}{2}\phi_{\mathbf{k}}\left(k_x^2 + k_y^2 + \eta k_z^2\right)\phi_{-\mathbf{k}}, \tag{A5}$$

$$S_e = \int d^4x\ ie\phi\psi^\dagger\psi, \tag{A6}$$

where $H_l(m=0)$ is the Hamiltonian in momentum space for the CQF as shown in the main text, i.e.,

$$H_l(m=0) = t_1\left(k_x^2 - k_y^2\right)\sigma_x + 2t_1 k_x k_y \sigma_y + t_3 k_z^2 \sigma_z. \tag{A7}$$

The Green's function of bosons and fermions can be easily derived by finding inversion of the free Hamiltonian matrix, which is written as G_b, G_f. In the following RG calculation, we fix the parameters in Eq. (A7) as $t_1 = t_3 = 1$ without loss of generality.

In the Wilsonian RG, integrating out the high-energy modes, will generate an effective action with a lower energy cutoff and new parameters, and then we try to recover the same energy cutoff by a scale transformation of all operators and time-space coordinates. We derive the RG equation from iteratively integrating momentum shells whose fermions are within momentum $Q_\perp \in (Qe^{-l}, Q)$ in a infinite cylinder geometry, where $l = \ln\Lambda/\Lambda_0 > 0$ is the RG running parameter. The cylinder form of the momentum shell is suitable to evaluate the Feynman amplitudes of symmetries in our model and the results are qualitatively the same with an equal-energy shell integral. Such geometry is utilized in various previous works on the correlation effects of Weyl systems [47]. Since the vertex corrections are zero due to Ward identity, there are only two Feynman diagrams related to corrections on self-energy, see Fig. 6. We calculate those two diagrams and compare the coefficients before each term with original field theory as

$$S = \int \psi^\dagger\left(i\omega\sigma_0 + \left(k_x^2 - k_y^2\right)\delta t_1\sigma_x + 2k_x k_y \delta t_1\sigma_y + k_z^2\delta t_3\sigma_z\right)\psi + \frac{1}{2}\phi\left(\eta_\phi\left(k_x^2 + k_y^2\right) + F_\eta k_z^2\right)\phi, \tag{A8}$$

where integral measure is omitted and the momentum cutoff in the $k_x k_y$ plane is assumed to be unity in the calculation (i.e., the flowing parameters are taken as dimensionless ones implicitly). $\delta t_1, \delta t_3, \eta_\phi, F_\eta$ are four terms derived from the two Feynman amplitudes in Fig. 6. For example, the amplitude for (a) is $F_a(\boldsymbol{k}) = -e^2\int_{\text{shell}} d\boldsymbol{q}\ \text{Tr}(G_f(\boldsymbol{q}+\boldsymbol{k}/2)G_f(\boldsymbol{q}-\boldsymbol{k}/2))$ (the frequency part in this formula is absorbed into the four-vector of momentum $\boldsymbol{q}$). And the corresponding term η_ϕ is defined as $\eta_\phi = d^2F_a(\boldsymbol{k})/dk_x^2$, other terms are similar to derive in Eq. (A8), and it is straightforward to check that no other terms apart from the four in Eq. (A8) can be generated by RG with the same order.

The key part in RG is the scaling dimension analysis. As we mentioned in the main text, though CQFs disperse quadratically in three directions, there is still anisotropy in the three spatial directions. Therefore, we set the scaling dimension for time-space as $[\omega] = 1$, $[k_{x,y}] = z_1$, and $[k_z] = z_3$. The tree-level values of them are $z_1 = \frac{1}{2}$ and $z_3 = \frac{1}{2}$. To make our field theory controllable, we introduce the dimensional regularizations like scheme; specifically, we treat the spatial dimension in $k_x k_y$ plane as $3-\epsilon$ dimensions, where $\epsilon = 1$ corresponds to the realistic case here. Overall, the RG is in dimension $4-\epsilon+1$ where $4-\epsilon$ is the spatial dimension and 1 is the time dimension. Such a scheme is the result of the momentum shell geometry, namely, one can only add fictitious dimensions into the sphere integral part in the momentum-shell RG. That is to say, we only begin to consider the dimension after we integrate out the frequency and k_z freedoms. Under this conjecture of the dimensions, we can further derive the scaling dimension for field operators and get their tree-level values.

The scaling dimensions are thus $[\eta] = 2z_1 - 2z_3 - \eta_\phi$, $[e] = -z_3/2 + 1/2 - \eta_\phi/2 - (1-\epsilon)z_1/2$, $[t_1] = 1 - 2z_1$, $[t_3] = 1 - 2z_3$. (At tree level in 3D, we have $[\eta] = 0, [e] = 1/4, [t_1] = 0, [t_3] = 0$.) We obtain z_1, z_3 by requiring $t_1 = t_3 = 1$ fixed (flow equation for t_i equal zero). Such requirements leave us two equations:

$$z_1 = (1+\delta t_1)/2, \quad z_3 = (1+\delta t_3)/2. \tag{A9}$$

The remaining RG equations are

$$\frac{de}{dl} = (-z_3/2 + 1/2 - \eta_\phi/2 - (1-\epsilon)z_1/2)e, \quad \frac{d\eta}{dl} = (2z_1 - 2z_3 - \eta_\phi)\eta + F_\eta. \tag{A10}$$

The terms occuring in Eqs. (A10) as mentioned before can be derived from the two simple Feynman amplitudes. The analytical form of them are (we have already taken the momentum cutoff as unity for simplicity)

$$\delta t_1(\eta,\epsilon,e) = \frac{e^2\pi^{-2-\frac{\epsilon}{2}}}{64\eta^4\Gamma\left(\frac{3-\epsilon}{2}\right)}\left(\frac{3\pi^{3/2}\eta^{9/2}(5+2\eta^2+\eta^4)}{(1+\eta^2)^{5/2}} + 4\eta\Gamma\left(-\frac{5}{4}\right)\Gamma\left(\frac{7}{4}\right){}_3F_2\left(\frac{3}{2},\frac{7}{4},2;\frac{1}{2},\frac{9}{4};-\frac{1}{\eta^2}\right) - 12\Gamma\left(-\frac{7}{4}\right)\Gamma\left(\frac{9}{4}\right){}_3F_2\left(2,\frac{9}{4},\frac{5}{2};\frac{3}{2},\frac{11}{4};-\frac{1}{\eta^2}\right)\right),$$

$$\delta t_3(\eta,\epsilon,e)=\frac{e^2\pi^{-2-\frac{\epsilon}{2}}}{16\eta^3\Gamma\left(\frac{3-\epsilon}{2}\right)}\left(-\frac{10\pi^{3/2}\eta^{11/2}}{(1+\eta^2)^{5/2}}+\frac{2\pi^{3/2}\eta^{15/2}}{(1+\eta^2)^{5/2}}-12\eta^2\Gamma\left(\frac{3}{4}\right)^2{}_3F_2\left(\frac{3}{4},\frac{3}{2},2;\frac{1}{2},\frac{5}{4};-\frac{1}{\eta^2}\right)\right.$$
$$\left.-\eta\Gamma\left(-\frac{3}{4}\right)\Gamma\left(\frac{5}{4}\right){}_3F_2\left(\frac{5}{4},\frac{3}{2},2;\frac{1}{2},\frac{7}{4};-\frac{1}{\eta^2}\right)\right)$$
$$+\frac{e^2\pi^{-2-\frac{\epsilon}{2}}}{16\eta^3\Gamma\left(\frac{3-\epsilon}{2}\right)}\left(48\eta\Gamma\left(\frac{5}{4}\right)^2{}_3F_2\left(\frac{5}{4},2,\frac{5}{2};\frac{3}{2},\frac{7}{4};-\frac{1}{\eta^2}\right)+3\Gamma\left(-\frac{5}{4}\right)\Gamma\left(\frac{7}{4}\right){}_3F_2\left(\frac{7}{4},2,\frac{5}{2};\frac{3}{2},\frac{9}{4};-\frac{1}{\eta^2}\right)\right),$$
$$\eta_\phi(\epsilon,e)=\frac{0.0274e^2\pi^{\frac{1-\epsilon}{2}}}{\Gamma\left(\frac{3-\epsilon}{2}\right)},$$
$$F_\eta(\epsilon,e)=\frac{0.01073e^2\pi^{\frac{1-\epsilon}{2}}}{\Gamma\left(\frac{3-\epsilon}{2}\right)},\tag{A11}$$

where η is the anisotropy character of Coulomb interaction, ϵ is the small parameter from dimension expansion, e is the Coulomb coupling strength, Γ is the conventional Gamma function, and ${}_3F_2$ is the generalized hypergeometric function. Note the numerical value is already evaluated if there is no complicated function and parameters dependence on η. Practically, the dimensional parameter ϵ is only taken for the integral of polar angles part since the set of gamma matrices and hence the exact dispersion relations are not well defined on arbitrary dimensions. The same approach for dimension consideration is also explored in various works on correlation effects of Fermi-point systems [55,56].

By numerically iterating the above flow equations, we find the unique stable fixed point $(\eta, e)\approx(0.66, 4.1)$ with finite interaction strength ($e\neq 0$) and anisotropy for Coulomb potentials $\eta\neq 1$ when $\epsilon=1$, namely, in 3D space. In this stable fixed point, $z_1\approx 0.639$, $z_3\approx 0.546$, which is not far from the free value, indicating that such a fixed point is under control in the RG sense. To clarify the stableness of such a fixed point and the control scheme by dimensional trick, we further analyze the fixed point from the marginal dimension and lower the dimension from $\epsilon=0$ to $\epsilon=1$.

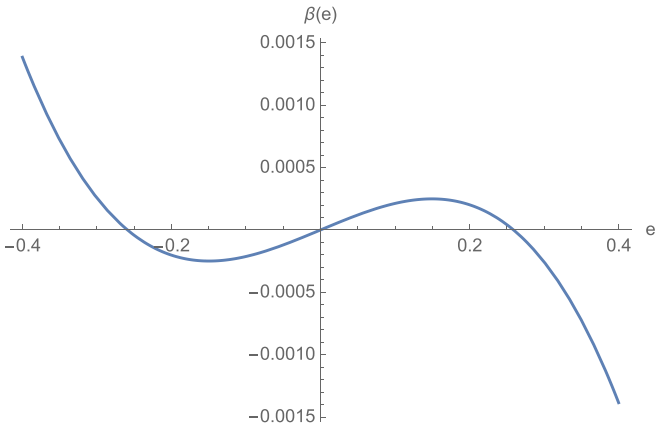

FIG. 7. The beta function plot of Coulomb coupling when $\epsilon=0.01$, the rightmost zero node is clearly a stable one with nonvanishing e correspoding to NFL states while the middle one is an unstable Gaussion fixed point.

When $\epsilon=0$, Coulomb interaction is marginally irrelevant, there is a stable noninteracting fixed point ($e=0$, $\eta\approx 0.66$) in such settings and the pure Gaussian one with isotropic screening $\eta=1$ is unstable toward the stable one when Coulomb interactions turns on at the beginning, though e finally flows to zero due to the marginal irrelevance. By lowering the dimensions with increasing ϵ, the stable Coulomb interacting NFL fixed point naturally moves away from the noninteracting one. For $\epsilon=0.01$, the plot of beta function for Coulomb coupling e is shown as Fig. 7 ($\eta=0.66$). It can be shown that the stable fixed point with Coulomb interaction is moving with increasing e when lowering the dimensions. The stable fixed point when $\epsilon=0.01$ is very close to the Gaussian one, and the scaling dimension on this fixed point is $z_1=0.5011$, $z_3=0.5004$; it is clear the shift of these values from their non-interacting values is controlled by the small parameter ϵ and thus justify the existence of the stable fixed point in 3D.

As a side note, there is another term as $t_s(k_x^2+k_y^2)\sigma_z$ which is also symmetry allowed in the effective Hamiltonian for

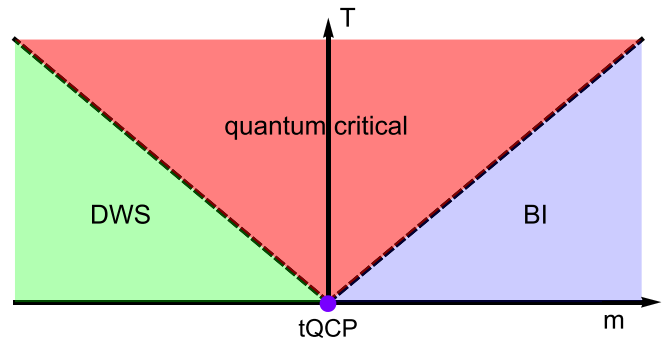

FIG. 8. Generic finite-temperature phase diagram for quantum phase transitions in 3D systems with double-Weyl fermions: The critical quadratic Weyl fermions (CQFs) emerge at the QCP with $m=0$. The finite-temperature crossover is described by the dashed lines and controlled by CQF at the QCP. The three regimes show characteristic behaviors in physical quantities. For instance, the specific heat shows $C\sim e^{-|m|/T}$ in the insulator phase, $C\sim T^2$ along with exotic logarithmic corrections in the double-Weyl SM phase, and $C\sim T^{1.82}$ in the quantum critical regime which shows non-Fermi liquid behavior.

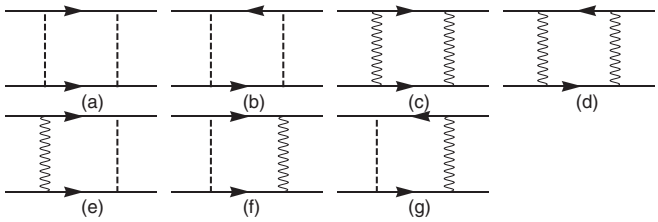

FIG. 9. Feynman diagrams contribute to four-fermion interactions: Solid lines stand for fermions, wavy lines stand for Coulomb potential, and dashed lines stand for short-range interaction.

low-energy fermions. We omit this term when we transform the lattice model to the effective theory for CQF. We here justify the omission of this term. The β function for this term is $dt_s/dl = (1 - 2z_1)t_s + \delta t_s \approx -0.3t_s + 0.01$, where we have replaced those parameter by values on the stable fixed point; namely, although t_s can be generated though its bare value vanishes, we can still treat it as zero safely. Because t_s is irrelevant with a negative scaling dimension and also the stable t_s is very small, we believe it has no qualitative modifications on the RG picture above.

We also mention some physical consequences here for this stable fixed point. We investigate the effect of finite $\eta \neq 1$ by RPA analysis. The particle-hole polarization with a propagator for CQFs gives numerical results as

$$\Pi(q_\perp) \propto q_\perp^2, \quad \Pi(q_z) \propto q_z^2 \tag{A12}$$

when the momentum transfer is small. The power-law behaviors are the same in different directions in the CQF case while there are different power laws in different directions in double-Weyl fermions. The only anisotropy in particle-hole polarization appears in the coefficients before momenta, namely, we have the full polarization as

$$-\Pi(\boldsymbol{q}) \approx a q_\perp^2 + b q_z^2, \tag{A13}$$

here $a \neq b$ represents the anisotropy in CTWF which is a weaker type of anisotropy compared to triple-Weyl fermions. Moreover, the renormalized Coulomb potential in this case behaves as $V(\boldsymbol{q}) = \frac{1}{q_\perp^2 + q_z^2 - \Pi(\boldsymbol{q})} \propto \frac{1}{c q_\perp^2 + q_z^2}$, where $c \neq 1$ shows the anisotropy in Coulomb interactions. By Fourier transformations into real space, Coulomb potential behaves as

$$V(\boldsymbol{r}) \propto \frac{1}{\sqrt{r_\perp^2 + c r_z^2}}. \tag{A14}$$

The long-range behaviors of renormalized Coulomb potential together with the finite g at the NFL fixed point show that Coulomb interactions receive no effective screening and actually drive the system to a NFL critical phase with finite interactions and the remaining anisotropy for Coulomb potential shows the difference between CQF here and 3D QBT systems given by Luttinger Hamiltonian.

In NFL states, various physical observables scale with exotic power laws. As for specific heat, consider the free CQF without Coulomb interactions—its specific heat can be

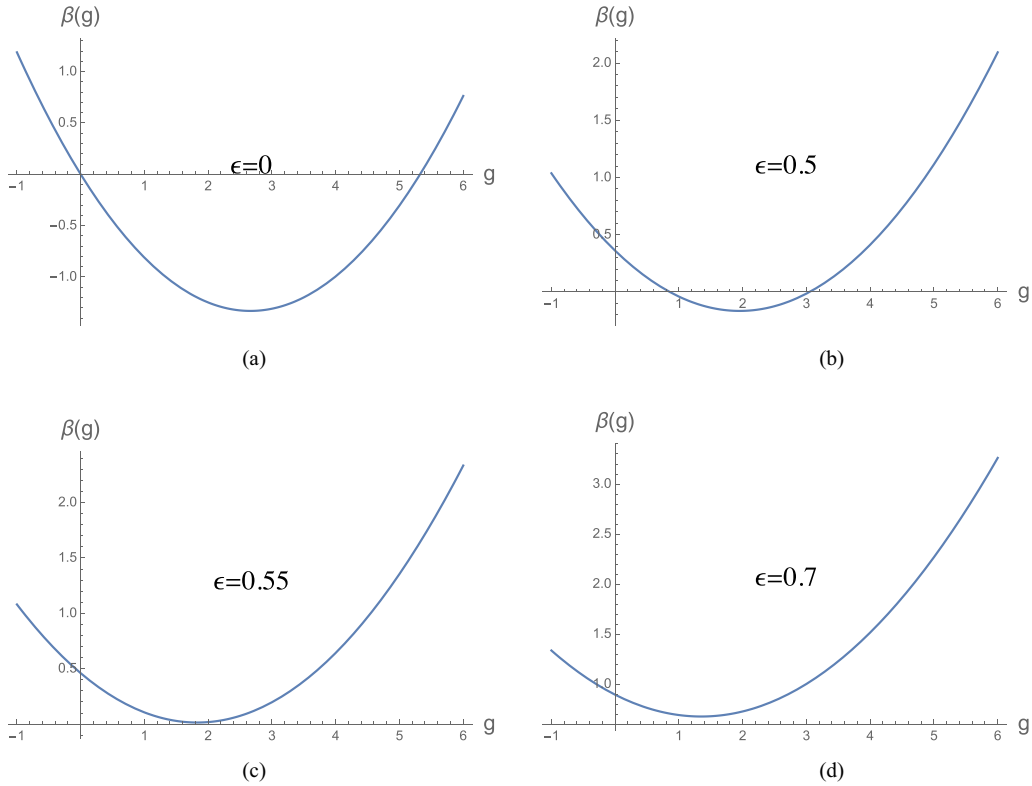

FIG. 10. The beta functions of short-range interaction g in $d = 4, 3.5, 3.45, 3.3$ dimensions with $\eta = 0.66$ and e corresponding to individual fixed values, respectively. In cases (a) and (b), the left zero nodes correspond to stable (IR) fixed points while the right ones correspond to the unstable one (UV). In case (c), the two fixed points merge, and there is only one stable fixed point. This happens when $d = d_c$. In case (d), $d < d_c$, there is no fixed point, and the short-range interaction flows to positive infinity as expected.

deduced by densities of states near Weyl nodes $\rho(\epsilon) \sim \epsilon^{1/2}$, which behaves as $C \sim T^{3/2}$. When Coulomb interactions are taken into consideration, NFL behaviors emerge where scaling dimensions z_1, z_3 get modifications from tree-level value and specific heat in the interacting case scales as an exotic power law:

$$C \sim T^{2z_1+z_3} \sim T^{1.82}. \tag{A15}$$

In sum, the topological QCP picture is slightly modified by Coulomb interactions when short-range interactions are negligible (less than the critical value g_c mentioned in the last section), as illustrated in Fig. 8.

3. RG analysis on CQF with both Coulomb and short-range interactions

In this Appendix section, we include both long-range interaction e as well as short-range interaction g into the full action Eq. (A3) and perform equal-footing renormalization analysis to see how the interplay between long-range and short-range interactions affects the physics picture we originally assumed. Again, we use the dimensional technique in these analysis to regulate the field theory and make the results more convincing. The scaling dimension of short-range coupling $[g] = -2z_1 - z_3 - (1-\epsilon)z_1 + 1$, in tree level, $[g] = -1/2$ in 3D.

The calculation is similar with the case above except the short-range interactions in this part. So we only focus on the renormalization for short-range interactions in this section. There are very limit diagrams with nonvanishing amplitudes for four-fermion interactions and they are listed as Fig. 9. One can check that other diagrams give zero amplitudes due to symmetry reasons. Remember that we choose only one independent interaction $g(\psi^\dagger\psi)^2$, and once we meet other forms of interactions, we should transform them back to g using Fierz identity in each RG step. The only difference compared to the last section is the inclusion of the beta function for g,

$$\frac{dg}{dl} = (1 - 2z_1 - z_3 - (1-\epsilon)z_1)g + F_1 g^2 + F_2 g e^2 + F_3 e^4, \tag{A16}$$

here F_i are calculated from Feynman amplitudes as Fig. 9. [Figures 9(a) and 9(b) contribute to F_1, Figs. 9(c) and 9(d) contribute to F_3, and Figs. 9(e)–9(g) contribute to F_2]. The existence of Figs. 9(c) and 9(d) tells us Coulomb interactions can drive out short-range interactions even when its bare value is zero. That is the key of the breakdown of the conventional picture referring to this type of topological phase transition. The flow diagram in this case is shown in the main text.

To compute these F terms, we let the momentum of all outer lines of the diagrams be zero. For example, $M_1 = -2\int_{\text{shell}} d\boldsymbol{q} G_f(\boldsymbol{q})G_f(-\boldsymbol{q}) - 2\int_{\text{shell}} d\boldsymbol{q} G_f(\boldsymbol{q})G_f(\boldsymbol{q})$, again, we absorb the frequency part into $\boldsymbol{q}$. Note the result M_1 is a matrix; we need to transform it back as an identity matrix using Fiertz identity, then the constant before the identity matrix is the value of F_1 we want, i.e., $M_1 = F_1 I$. The specific form of the three F terms from Feynman amplitudes is shown below:

$$\begin{aligned}
F_1(\epsilon) &= \frac{0.1665\pi^{-\frac{\epsilon}{2}}}{\Gamma\left(\frac{3-\epsilon}{2}\right)},\\
F_2(\eta,\epsilon) &= \frac{\pi^{-2-\frac{\epsilon}{2}}}{4\eta^2\sqrt{1+\eta^2}\Gamma\left(\frac{3-\epsilon}{2}\right)}\left(\pi^{3/2}\eta^{5/2} + \eta\sqrt{1+\eta^2}\Gamma\left(\frac{3}{4}\right)^2 {}_2F_1\left(\frac{3}{4},1;\frac{1}{4};-\frac{1}{\eta^2}\right) - 4\sqrt{1+\eta^2}\Gamma\left(\frac{5}{4}\right)^2 {}_2F_1\left(1,\frac{5}{4};\frac{3}{4};-\frac{1}{\eta^2}\right)\right)\\
&\quad + \frac{\pi^{-2-\frac{\epsilon}{2}}}{4\eta^2\sqrt{1+\eta^2}\Gamma\left(\frac{3-\epsilon}{2}\right)}\left(-4\eta\sqrt{1+\eta^2}\Gamma\left(\frac{3}{4}\right)\Gamma\left(\frac{7}{4}\right){}_2F_1\left(1,\frac{7}{4};\frac{5}{4};-\frac{1}{\eta^2}\right)\right.\\
&\quad \left. - \sqrt{1+\eta^2}\Gamma\left(-\frac{3}{4}\right)\Gamma\left(\frac{9}{4}\right){}_2F_1\left(1,\frac{9}{4};\frac{7}{4};-\frac{1}{\eta^2}\right)\right),\\
F_3(\eta,\epsilon) &= \frac{\pi^{-2-\frac{\epsilon}{2}}}{32\Gamma\left(\frac{3-\epsilon}{2}\right)}\left(2\sqrt{\pi}\left(-\frac{3\pi\left(1-\frac{1}{\eta^2}\right)}{2\left(\frac{1}{\eta}+\eta\right)^{5/2}} - \frac{2\Gamma\left(-\frac{1}{4}\right)\Gamma\left(\frac{7}{4}\right){}_2F_1\left(\frac{7}{4},2;\frac{5}{4};-\frac{1}{\eta^2}\right)}{\sqrt{\pi}\eta^3} + \frac{4\Gamma\left(\frac{5}{4}\right)^2{}_3F_2\left(1,\frac{5}{4},\frac{3}{2};\frac{1}{2},\frac{3}{4};-\frac{1}{\eta^2}\right)}{\sqrt{\pi}\eta^2}\right)\right)\\
&\quad + \frac{\pi^{-2-\frac{\epsilon}{2}}}{32\Gamma\left(\frac{3-\epsilon}{2}\right)}\left(\frac{\frac{\pi^{3/2}\eta^{11/2}(7+\eta^2)}{(1+\eta^2)^{5/2}} - 4\Gamma\left(-\frac{5}{4}\right)\Gamma\left(\frac{11}{4}\right){}_2F_1\left(2,\frac{11}{4};\frac{9}{4};-\frac{1}{\eta^2}\right) + 2\eta\Gamma\left(-\frac{3}{4}\right)\Gamma\left(\frac{9}{4}\right){}_3F_2\left(1,1.5,\frac{9}{4};\frac{1}{2},\frac{7}{4};-\frac{1}{\eta^2}\right)}{\eta^3}\right),
\end{aligned} \tag{A17}$$

where ${}_iF_j$ is a generalized hypergeometric function.

After obtaining all terms in the flow equation, we can numerically iterate the flow equations and obtain the RG flow diagram as in the main text, which clearly shows the relevance of short-ranged interactions.

Observe the flow for different dimensions ϵ, we can further see how the fixed point is shifted in a controlled way by the dimensions. When $\epsilon = 0$, the scaling dimension for the short-range interaction on the interacting fixed point of Coulomb interaction is $[g] = -1$ and is thus still irrelevant in the upper critical dimension $d = 4$. Therefore, the proposed scenario occurs below some critical dimension $d_c = 4 - \epsilon_c$. The shift of g from irrelevance to relevance is still well captured by the dimension-lowering process and is thus controllable as

shown below. The similar picture and RG arguments through dimensional technique also occurs in 3D QBT systems with cubic symmetry [55], where no anisotropic screening effect sets in.

We investigate how the fixed point shifts when spatial dimension is lowering. To show this, we draw several beta function plots with e, η values at a stable fixed point from the last section while varying g, since g cannot change the behavior of the long-range interaction part as the value doesn't enter the flow equation for e and η at least in one loop level. So, it is sufficient to study the flow along the line across the interacting so-called NFL fixed point of Coulomb interaction with a varying short-range interaction. We can see the detail of the shift in Fig. 10. As we can see, when $\epsilon = 0$, the $g = 0$ fixed point is stable. When $\epsilon > 0$, this stable fixed point shifts to $g > 0$ and the system has a fixed point with both finite g and e. After $d = d_c$, which is estimated as $d \approx 0.45$, the stable fixed point is merged with the UV fixed point, leaving a flow to infinity of g below the critical dimension. It is worth noting the critical dimension obtained here, $d_c \approx 3.45$, is larger than the case in Ref. [55], implying that our system is of higher possibility, showing strong short-ranged interactions in real dimension $d = 3$.

There is still a slight possibility that $\epsilon_c > 1$ when contributions from higher loops are seriously considered, but this task is beyond the reach of the current paper. However, even if $d_c < 3$, it is still in the middle phase in Fig. 10(b) in 3D. In such a case, the finite g on the stable fixed point is still enough ($g > g_c$) to drive the nematic phase transition with high probability—namely, the short-range interaction is not necessarily leading to infinite, a stable fixed point with finite g strength $g > g_c$ is enough to induce the nematic order. Based on the discussions and arguments using dimensional technique, we are confident the physical scenario in three spatial dimensions is that the putative critical point of Coulomb interaction is preempted by a nematic phase induced by strong short-range interactions.

4. RG near the QCP: Double-Weyl fermions with both interactions

As explained in the main text, we use an effective theory for double-Weyl fermions to investigate behaviors around but not exactly at the QCP, and we use the implicitly assumed cutoff in the action as the control parameter which tunes the separation of two double-Weyl nodes in crystal momentum space: $\Lambda \sim \sqrt{m}$. All the above RG procedures still apply to the double-Weyl fermion case, in principle, as long as we replace the propagator for CQF with double-Weyl fermions. And note this time we cannot simply set cutoff Λ to be unity. Instead, we need to vary Λ to study the scaling behavior for phase boundaries around the QCP.

The first observation is the existence of critical e^*. Coulomb interactions are marginally irrelevant in the double-Weyl fermion case, which means infinitesimal Coulomb interactions cannot drive short-range interactions leaving the system in the double-Weyl fermion phase. However, Coulomb interaction exceeding e^* can still lead to runaway flow of on-site interactions. This picture can be directly shown from the flow diagram Fig. 11.

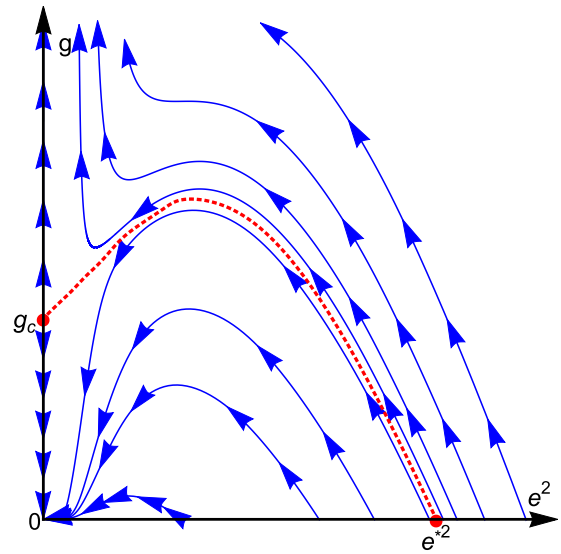

FIG. 11. Flow diagrams for double-Weyl fermions with both types of interactions: The red dotted line stand for the phase boundary between double-Weyl fermions and nematic phases determined by RG.

There is other information in the flow diagram. Even if $e < e^*$, Coulomb interaction is also helpful to enhance the short-range interaction g, namely, the critical value g_c is still finite when $0 < e < e^*$, while it is less than the mean-field critical value now. According to the red line, we come to the conclusion $0 = g_c(e \geqslant e^*) < g_c(0 < e < e^*) < g_c(e = 0) = g_c$ in a wide parameter range.

Furthermore, we explore the scaling relations between those phase boundaries and cutoff representing the separation of double-Weyl nodes. First, we can show $e^{*2}(|m|) \sim \sqrt{|m|}$—namely, as two double-Weyl nodes leave each other, the critical e to drive out on-site interactions becomes larger. This is consistent with the CQF limit ($m = 0$), where we can treat it as $e^* = 0$ (infinitesimal Coulomb interaction is enough to drive short-range interactions). Now consider cases with finite fixed e, due to the relation $e^{*2} = \sqrt{|m|/C'}$ (C' is just a constant), we have the critical $|m|_c = C' e^4$. And the system is at the nematic phase even if there is no bare on-site interaction when $0 < |m| < |m|_c$. When $|m| > |m|_c$, e is now less than $e^*(|m|)$, however, based on the above observation, $g_c(m)$ is still less than its mean-field value. Numerical results show the scaling behavior here is $g_c \sim \sqrt{|m|} - \sqrt{|m|_c}$ when m is slightly larger than m_c.

Based on all the above results, we obtain the illustrative phase diagram for the model in the main text. It is worth noting that the RG calculations and approaches in this Appendix section are not so strict in the field theory sense since both types of interactions are irrelevant at tree level. This section thus serves as a further exploration beyond the results we obtained exactly on the critical point and might provide useful insights on the behavior in double-Weyl fermion phases.

[1] S. L. Sondhi, S. M. Girvin, J. P. Carini, and D. Shahar, Rev. Mod. Phys. **69**, 315 (1997).

[2] S. Sachdev, *Quantum Phase Transitions* (Cambridge University Press, Cambridge, 2011).

[3] I. Herbut, *A Modern Approach to Critical Phenomena* (Cambridge University Press, New York, 2007).

[4] H. v. Lohneysen, A. Rosch, M. Vojta, and P. Wolfle, Rev. Mod. Phys. **79**, 1015 (2007).

[5] G. R. Stewart, Rev. Mod. Phys. **73**, 797 (2001).

[6] G. R. Stewart, Rev. Mod. Phys. **78**, 743 (2006).

[7] L. Taillefer, Annu. Rev. Condens. Matter Phys. **1**, 51 (2010).

[8] T. Shibauchi, A. Carrington, and Y. Matsuda, Annu. Rev. Condens. Matter Phys. **5**, 113 (2014).

[9] A. Abanov, A. V. Chubukov, and A. M. Finkelstein, Europhys. Lett. **54**, 488 (2001).

[10] R. Roussev and A. J. Millis, Phys. Rev. B **63**, 140504(R) (2001).

[11] Y. Huh and S. Sachdev, Phys. Rev. B **78**, 064512 (2008).

[12] T. Senthil, Phys. Rev. B **78**, 035103 (2008).

[13] M. A. Metlitski and S. Sachdev, New J. Phys. **12**, 105007 (2010).

[14] M. A. Metlitski and S. Sachdev, Phys. Rev. B **82**, 075127 (2010).

[15] M. A. Metlitski and S. Sachdev, Phys. Rev. B **82**, 075128 (2010).

[16] Y. Wang and A. V. Chubukov, Phys. Rev. Lett. **110**, 127001 (2013).

[17] A. L. Fitzpatrick, S. Kachru, J. Kaplan, S. Raghu, and G. Torroba, and H. Wang, arXiv:1410.6814.

[18] S. Ghamari, S.-S. Lee, and C. Kallin, Phys. Rev. B **92**, 085112 (2015).

[19] S. Lederer, Y. Schattner, E. Berg, and S. A. Kivelson, Phys. Rev. Lett. **114**, 097001 (2015).

[20] M. A. Metlitski, D. F. Mross, S. Sachdev, and T. Senthil, Phys. Rev. B **91**, 115111 (2015).

[21] A. Schlief, P. Lunts, and S.-S. Lee, Phys. Rev. X **7**, 021010 (2017).

[22] P. Lunts, A. Schlief, and S.-S. Lee, Phys. Rev. B **95**, 245109 (2017).

[23] M. Z. Hasan and C. L. Kane, Rev. Mod. Phys. **82**, 3045 (2010), and references therein.

[24] X.-L. Qi and S.-C. Zhang, Rev. Mod. Phys. **83**, 1057 (2011), and references therein.

[25] N. P. Armitage, E. J. Mele, and A. Vishwanath, Rev. Mod. Phys. **90**, 015001 (2018).

[26] X. Wan, A. M. Turner, A. Vishwanath, and S. Y. Savrasov, Phys. Rev. B **83**, 205101 (2011).

[27] G. Xu, H. Weng, Z. Wang, X. Dai, and Z. Fang, Phys. Rev. Lett. **107**, 186806 (2011).

[28] A. A. Burkov and L. Balents, Phys. Rev. Lett. **107**, 127205 (2011).

[29] P. Hosur and X. Qi, C. R. Phys. **14**, 857 (2013).

[30] B.-J. Yang and N. Nagaosa, Nat. Commun. **5**, 4898 (2014).

[31] C. Fang, M. J. Gilbert, X. Dai, and B. A. Bernevig, Phys. Rev. Lett. **108**, 266802 (2012).

[32] S.-M. Huang, S.-Y. Xu, I. Belopolski, C.-C. Lee, G. Chang, B. K. Wang, N. Alidoust, M. Neupane, H. Zheng, D. Sanchez, A. Bansil, G. Bian, H. Lin, and M. Z. Hasan, Proc. Natl. Acad. Sci. USA **113**, 1180 (2016).

[33] A. A. Soluyanov, D. Gresch, Z. Wang, Q. Wu, M. Troyer, X. Dai, and B. A. Bernevig, Nature **527**, 495 (2015).

[34] C.-K. Chiu, J. C. Y. Teo, A. P. Schnyder, and S. Ryu, Rev. Mod. Phys. **88**, 035005 (2016).

[35] B. Bradlyn, J. Cano, Z. Wang, M. G. Vergniory, C. Felser, R. J. Cava, and B. A. Bernevig, Science **353**, aaf5037 (2016).

[36] J. Ruan, S.-K. Jian, H. Yao, H. Zhang, S.-C. Zhang, and D. Xing, Nat. Commun. **7**, 11136 (2016).

[37] J. Ruan, S.-K. Jian, D. Zhang, H. Yao, H. Zhang, S.-C. Zhang, and D. Xing, Phys. Rev. Lett. **116**, 226801 (2016).

[38] R. Shankar, Rev. Mod. Phys. **66**, 129 (1994).

[39] I. F. Herbut, Phys. Rev. Lett. **97**, 146401 (2006).

[40] I. F. Herbut, V. Juričić, and B. Roy, Phys. Rev. B **79**, 085116 (2009).

[41] K. Sun, H. Yao, E. Fradkin, and S. A. Kivelson, Phys. Rev. Lett. **103**, 046811 (2009).

[42] Q. Liu, H. Yao, and T. Ma, Phys. Rev. B **82**, 045102 (2010).

[43] W.-F. Tsai, C. Fang, H. Yao, and J. Hu, New J. Phys. **17**, 055016 (2015).

[44] J. Maciejko and R. Nandkishore, Phys. Rev. B **90**, 035126 (2014).

[45] L. Savary, E.-G. Moon, and L. Balents, Phys. Rev. X **4**, 041027 (2014).

[46] J. M. Murray, O. Vafek, and L. Balents, Phys. Rev. B **92**, 035137 (2015).

[47] B. Roy, P. Goswami, and V. Juricic, Phys. Rev. B **95**, 201102(R) (2017).

[48] P. Goswami and S. Chakravarty, Phys. Rev. Lett. **107**, 196803 (2011).

[49] H. Isobe and N. Nagaosa, Phys. Rev. B **86**, 165127 (2012).

[50] H. Isobe and N. Nagaosa, Phys. Rev. B **87**, 205138 (2013).

[51] A. A. Abrikosov and S. D. Beneslavskii, Sov. Phys. JETP **32**, 699 (1971).

[52] A. A. Abrikosov, Sov. Phys. JETP **39**, 709 (1974).

[53] E.-G. Moon, C. Xu, Y. B. Kim, and L. Balents, Phys. Rev. Lett. **111**, 206401 (2013).

[54] S. Han and E.-G. Moon, Phys. Rev. B **97**, 241101(R) (2018).

[55] I. F. Herbut and L. Janssen, Phys. Rev. Lett. **113**, 106401 (2014).

[56] L. Janssen and I. F. Herbut, Phys. Rev. B **92**, 045117 (2015).

[57] L. Janssen and I. F. Herbut, Phys. Rev. B **93**, 165109 (2016).

[58] L. Janssen and I. F. Herbut, Phys. Rev. B **95**, 075101 (2017).

[59] A. A. Abrikosov, J. Low Temp. Phys. **8**, 315 (1972).

[60] B.-J. Yang, E.-G. Moon, H. Isobe, and N. Nagaosa, Nat. Phys. **10**, 774 (2014).

[61] H. Isobe, B.-J. Yang, A. Chubukov, J. Schmalian, and N. Nagaosa, Phys. Rev. Lett. **116**, 076803 (2016).

[62] S.-K. Jian and H. Yao, Phys. Rev. B **92**, 045121 (2015).

[63] H.-H. Lai, Phys. Rev. B **91**, 235131 (2015).

[64] S.-X. Zhang, S.-K. Jian, and H. Yao, Phys. Rev. B **96**, 241111(R) (2017).

[65] S. Han, G. Y. Cho, and E.-G. Moon, Phys. Rev. B **98**, 085149 (2018).

[66] Z.-X. Li, Y.-F. Jiang, S.-K. Jian, and H. Yao, Nat. Commun. **8**, 314 (2017).

[67] S.-K. Jian and H. Yao, Phys. Rev. B **96**, 155112 (2017).

[68] S.-K. Jian and H. Yao, Phys. Rev. B **96**, 195162 (2017).

[69] M. M. Scherer and I. F. Herbut, Phys. Rev. B **94**, 205136 (2016).

[70] L. Classen, I. F. Herbut, and M. M. Scherer, Phys. Rev. B **96**, 115132 (2017).

[71] E. Torres, L. Classen, I. F. Herbut, and M. M. Scherer, Phys. Rev. B **97**, 125137 (2018).

[72] S.-S. Lee, Phys. Rev. B **76**, 075103 (2007).

[73] Y. Yu and K. Yang, Phys. Rev. Lett. **105**, 150605 (2010).
[74] T. Grover, D. N. Sheng, and A. Vishwanath, Science **344**, 280 (2014).
[75] P. Ponte and S.-S. Lee, New J. Phys. **16**, 013044 (2014).
[76] S.-K. Jian, Y.-F. Jiang, and H. Yao, Phys. Rev. Lett. **114**, 237001 (2015).
[77] S.-K. Jian, C.-H. Lin, J. Maciejko, and H. Yao, Phys. Rev. Lett. **118**, 166802 (2017).
[78] Z.-X. Li, A. Vaezi, C. B. Mendl, and H. Yao, Sci. Adv. **4**, eaau1463 (2018).
[79] H. Weyl, Z. Phys. **56**, 330 (1929).
[80] S.-Y. Xu, I. Belopolski, N. Alidoust, M. Neupane, G. Bian, C. Zhang, R. Sankar, G. Chang, Z. Yuan, C.-C. Lee, S.-M. Huang, H. Zheng, J. Ma, D. S. Sanchez, B. Wang, A. Bansil, F. Chou, P. P. Shibayev, H. Lin, S. Jia, and M. Z. Hasan, Science **349**, 613 (2015).
[81] B. Q. Lv, H. M. Weng, B. B. Fu, X. P. Wang, H. Miao, J. Ma, P. Richard, X. C. Huang, L. X. Zhao, G. F. Chen, Z. Fang, X. Dai, T. Qian, and H. Ding, Phys. Rev. X **5**, 031013 (2015).
[82] L. X. Yang, Z. K. Liu, Y. Sun, H. Peng, H. F. Yang, T. Zhang, B. Zhou, Y. Zhang, Y. F. Guo, M. Rahn, D. Prabhakaran, Z. Hussain, S. K. Mo, C. Felser, B. Yan, and Y. L. Chen, Nat. Phys. **11**, 728 (2015).
[83] B. Q. Lv, N. Xu, H. M. Weng, J. Z. Ma, P. Richard, X. C. Huang, L. X. Zhao, G. F. Chen, C. E. Matt, F. Bisti, V. N. Strocov, J. Mesot, Z. Fang, X. Dai, T. Qian, M. Shi, and H. Ding, Nat. Phys. **11**, 724 (2015).
[84] S.-Y. Xu, N. Alidoust, I. Belopolski, Z. Yuan, G. Bian, T.-R. Chang, H. Zheng, V. N. Strocov, D. S. Sanchez, G. Chang, C. Zhang, D. Mou, Y. Wu, L. Huang, C.-C. Lee, S.-M. Huang, B. Wang, A. Bansil, H.-T. Jeng, T. Neupert, A. Kaminski, H. Lin, S. Jia, and M. Zahid Hasan, Nat. Phys. **11**, 748 (2015).
[85] S. A. Kivelson, E. Fradkin, and V. J. Emery, Nature **393**, 550 (1998).
[86] J. M. Luttinger, Phys. Rev. **102**, 1030 (1956).
[87] X.-G. Wen, Rev. Mod. Phys. **89**, 041004 (2017).